

Article

# Experimental and Finite Element Analysis to Investigate the Vibration of Oblique-Stud Stator Frame in a Large Hydropower Generator Unit

Jianzhong Zhou <sup>1,2,\*</sup>, Xuanlin Peng <sup>1,2,\*</sup>, Ruhai Li <sup>1,2</sup>, Yanhe Xu <sup>1,2</sup>, Han Liu <sup>1,2</sup> and Diyi Chen <sup>3</sup>

<sup>1</sup> School of Hydropower and Information Engineering, Huazhong University of Science and Technology, Wuhan 430074, China; D201577803@hust.edu.cn (R.L.); yh\_xu@hust.edu.cn (Y.X.); liuhan\_703@163.com (H.L.)

<sup>2</sup> Hubei Key Laboratory of Digital Valley Science and Technology, Huazhong University of Science and Technology, Wuhan 430074, China

<sup>3</sup> Institute of Water Resources and Hydropower Research, Northwest A & F University, Yangling 712100, China; diyichen@nwsuaf.edu.cn

\* Correspondence: jz.zhou@hust.edu.cn (J.Z.); pengxl0924@hust.edu.cn.com (X.P.); Tel.: +86-027-8754-3217 (J.Z.); +86-159-7208-4426 (X.P.)

Received: 2 November 2017; Accepted: 12 December 2017; Published: 19 December 2017

**Abstract:** This paper presents an investigation on the undesirable vibration of an oblique-stud stator frame in a large hydropower generator by means of experimental and finite element (FE) analysis. First, field experimental tests were performed, and the results indicate that the main vibration component comes from electromagnetic factors. Then, a 2D-magnetic and 3D-mechanical FE model was developed to investigate the vibration of the stator frame under the action of electromagnetic forces. A set of contrast models was established to study the effects of different kinds of eccentricity and different structures. Based on the comparative analysis between the results of simulations and experimental tests, it can be inferred that the abnormal vibration is generated because of the lack of stiffness in the upper part of structure and the existence of dynamic eccentricity in the rotor–stator system. In addition, the structural simulation analysis shows that the flexible designed oblique-stud stator frame is relatively vulnerable against the electromagnetic forces.

**Keywords:** experimental vibration test; 2D-magnetic and 3D-mechanical coupled finite element (FE) model; oblique-stud stator frame; eccentricity

---

## 1. Introduction

As a crucial part of the rotor–stator system, stator frame is not only a mechanical load-bearing component but also a carrier of the electric generator, which means that it will be affected by multiple factors such as electromagnetic force from the rotating rotor, outward thermal expansion force from the stator core, hydraulic turbulence from the base and structural gravity simultaneously during the practical operation. Therefore, the study of vibration of stator frame is a complex multi-field coupling problem. Many studies have been done to investigate the vibration of stator in the past decades, which can be classified into two categories: theoretical research and engineering application. Theoretical research mainly includes mathematical modeling, structure characteristic calculation, and dynamic response predicting using analytic or numerical method [1–3]. Engineering application mainly focuses on the vibration analysis technique, fault diagnosis technology and elimination solution [4–6]. These studies show that the excessive vibration of stator frame caused by assembly error, improper design, manufacturing deviation or other reasons can result in structural noise, fatigue damage, even bolt cutting and other negative effects, which would seriously threaten the safety of the unit.

With the development of large scale hydropower generator, higher requirement of security and stability are proposed. A novel stator frame with fixed base and oblique-studs was widely adopted in large capacity and low speed unit for its low production costs and the advantage of using elastic deformation to counteract external forces, and the features of the stator frame can be characterized by large elasticity and small rigidity. The authors, to investigate the abnormal vibration occurred on the oblique-stud stator frame in a 250 MW hydropower generator, have carried out the experimental test under various operating conditions, and to further study the impact of the electromagnetic factors on vibration, a finite element (FE) analysis was performed.

The calculation of electromagnetic force is of key importance in the simulation. Lots of studies are by means of analytical method which is relied on an accurate result of the magnetic field. For example, Smith et al. described a method for predicting the static and pulsating unbalanced magnetic pull (UMP) in a three-phase, induction motor with an eccentric rotor [7,8]. Guo et al. [9] obtained an analytical expression of electromagnetic forces by expressing the air gap permeance as a Fourier series, but these methods are suitable for the initial design and optimization. When it comes to structure adjustment and dynamic response study, FE method is a better choice because it can provide more accurate result of the magnetic field by taking the saturation and complex structures into account. With the advent of the increased computational power, FE method has been widely used in engineering practice in the past several decades. However, there would be two big challenges for FE analysis of the stator frame in a large scale hydropower generator. Firstly, when investigating the electromagnetic effect of a rotating machine, eccentricity must be considered. The eccentricity would ruin the symmetry and periodicity of the structure, hence the conventional method that utilizing the symmetry and periodicity to simplify the computational model could no longer be used. Considering there are 64 magnetic poles, 528 coil slots and thousands of current sources in the studied stator model, the calculation would be very time-consuming. Secondly, it is difficult to find a coupling method of electromagnetic field and mechanical field with both high accuracy and acceptable calculating time. Fonteyn et al. proposed an approach which is referred as directly coupling method that is to solve the 2D magnetic field and calculate the displacement simultaneously without using the common “equivalent forces” approach, as in [10]. Lin and Arkkio [11] investigated the vibration of the end-windings on the stator by using an approach which is known as weakly coupling method: solving the electromagnetic field firstly and then utilizing the generated magnetic stress tensor as the boundary condition for the mechanical equations. To cut down the unacceptable computational time brought by the huge number of DOFs, Xu et al. [12] obtained the electromagnetic force by means of a simple analytical method that employed the no-load characteristic curve of an electrical machine, and then developed a FE rotor model of a large hydro-turbine generator unit to investigate the influence of UMP on radial vibrations. Matinez et al. [1] presented a 2D-magnetic and 3D-mechanical coupled FE model which is the most suitable method for the vibration study in the stator of induction motors, but it only focused on steady-state and the eccentric situation was not considered. Inspired by the work of [1], a 2D-magnetic and 3D-mechanical coupled FE model was developed in this paper. With different mechanical models, eccentricity and radial-stud structure were considered.

This work focuses on the vibration problem of an oblique-stud stator frame in a large scale hydropower generator. The field experimental tests, including excitation varying test, rotation speed varying test and load varying test, were carried out to find the cause of the undesirable vibration. To do a further mechanism study, a coupled FE model was established, and comparative analyses to reveal the relationship between vibration and structure were performed.

## 2. Field Experimental Tests

### 2.1. The Investigated Stator Frame

The stator frame was designed as a plate-like structure composed by rib-plates, annular-plates and oblique-studs (Figure 1) to dissipate heat and reduce the weight. Unlike the traditional radial-stud

structure, this stator frame uses an oblique-stud structure to reduce the deformation caused by thermal expansion. The research object is in a large hydropower generator unit which suffered stator vibration problem since it was put into operation. To find out the cause of the undesired vibration, experimental test and FE analysis were carried out, which is detailed in the following sections.

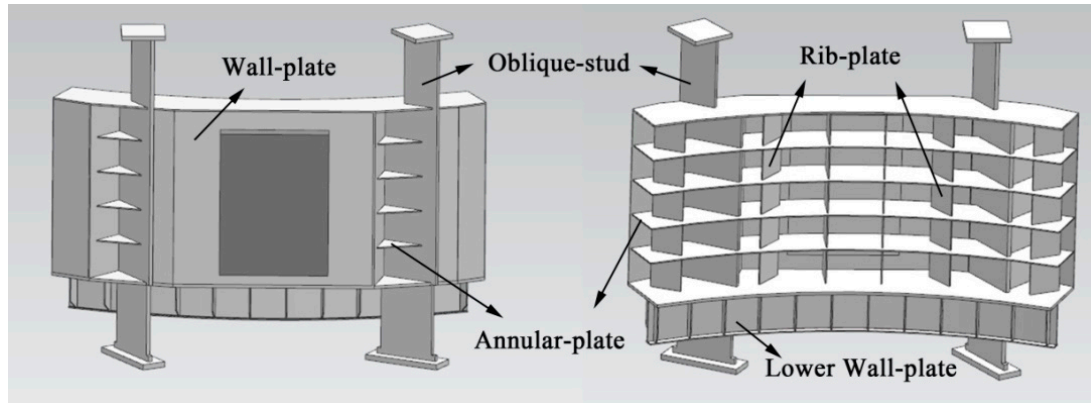


Figure 1. Structure diagram of the stator frame.

## 2.2. Three Sets of Experimental Tests

Since the hydropower unit is a complex hydraulic electromechanical coupling system, it is important to identify the main factor caused stator vibration at the first place. Three sets of field experimental tests were performed and the details are shown as follows:

Excitation varying tests at no-load condition: When the unit speeds up to the rated condition after start-up, a series of excitation with different excitation conditions (An increasing interval of 5% from 50% to 100% of the rated excitation current) are put into operation. When each operation condition turns into steady-state, the vibration data of the stator frame are collected.

Rotating speed varying tests at no-load condition: After the unit starting up to the rated condition, the rotating speed is adjusted to 94.3%, 99%, 102%, and 105% of the rated speed by manually setting the governor frequency. When each operation condition turns into steady-state, the vibration data of the stator frame are collected.

Load varying tests: After started up and installed, the unit is stabilized at different load conditions from the minimum load to the maximum load under the test head (20 MW to 250 MW), and the vibration data of each condition is collected respectively.

The vibration shape of the stator frame is elliptical deformation in the horizontal direction which is presented in Figure 2. Therefore, it is necessary to place monitoring points in the four directions (+X, -X, +Y, -Y) of the stator frame to measure the maximum amplitude of the vibration. Since the oblique-stud is the crucial supporting component of the stator system and its stiffness is large, eight low-frequency vibration sensors and ICP (VS-TH-DP, Hengyuan Hydropower Equipment Co., Shanxi province, Xi'an, China) acceleration sensors were set on upper portion (top and mid) of oblique-stud to collect the displacement and acceleration data of the structure (Figure 3). To ensure the accuracy of the experimental test, the sample frequency was set to 2.5 KHz and the sampling time was 89 s.

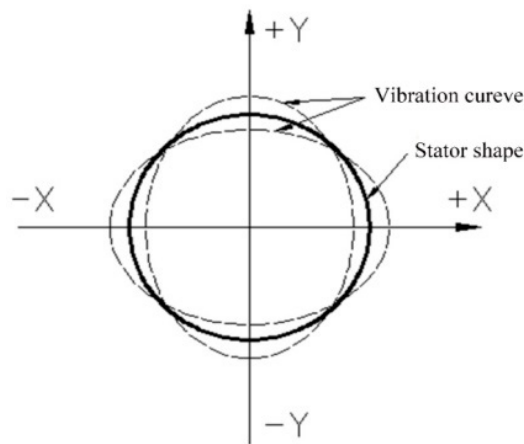


Figure 2. Vibration shape of the tested stator frame.

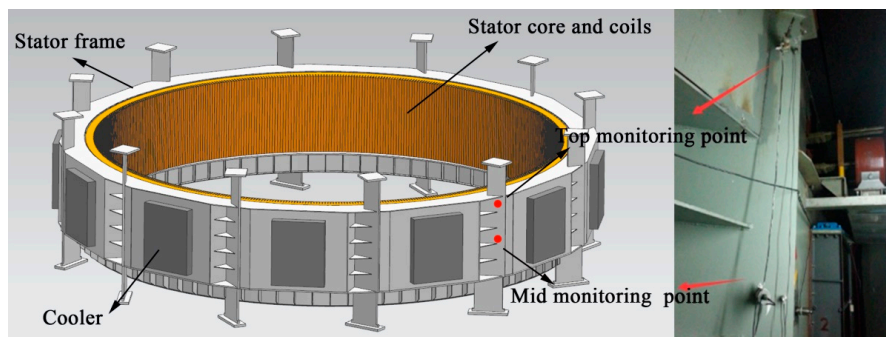


Figure 3. Diagram of monitoring point.

2.3. Results of the Experimental Tests

Figure 4 demonstrates the peak value of the displacement at the top and the mid of the stator frame in different experimental tests. It can be observed that the amplitude of vibration rises with the increasing excitation current, while it declines slightly with the increase of load, and there is no explicit relationship between vibration and rotation speed. It can also be found that the vibration at the mid part of the stator is obviously stronger than that at the top part.

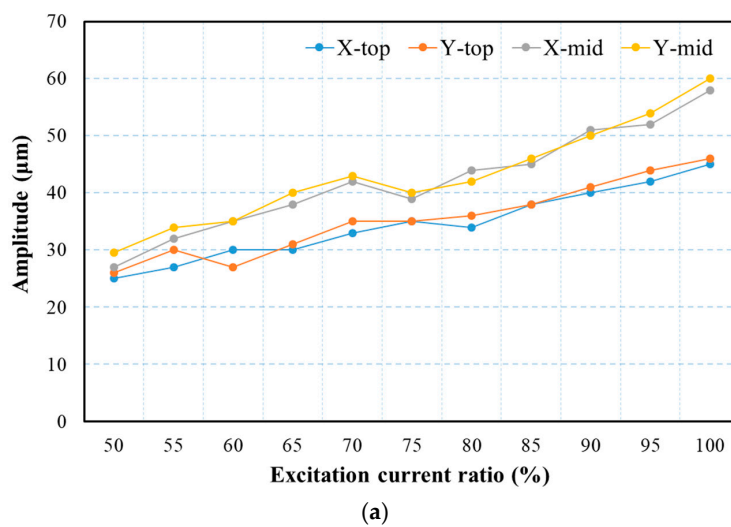
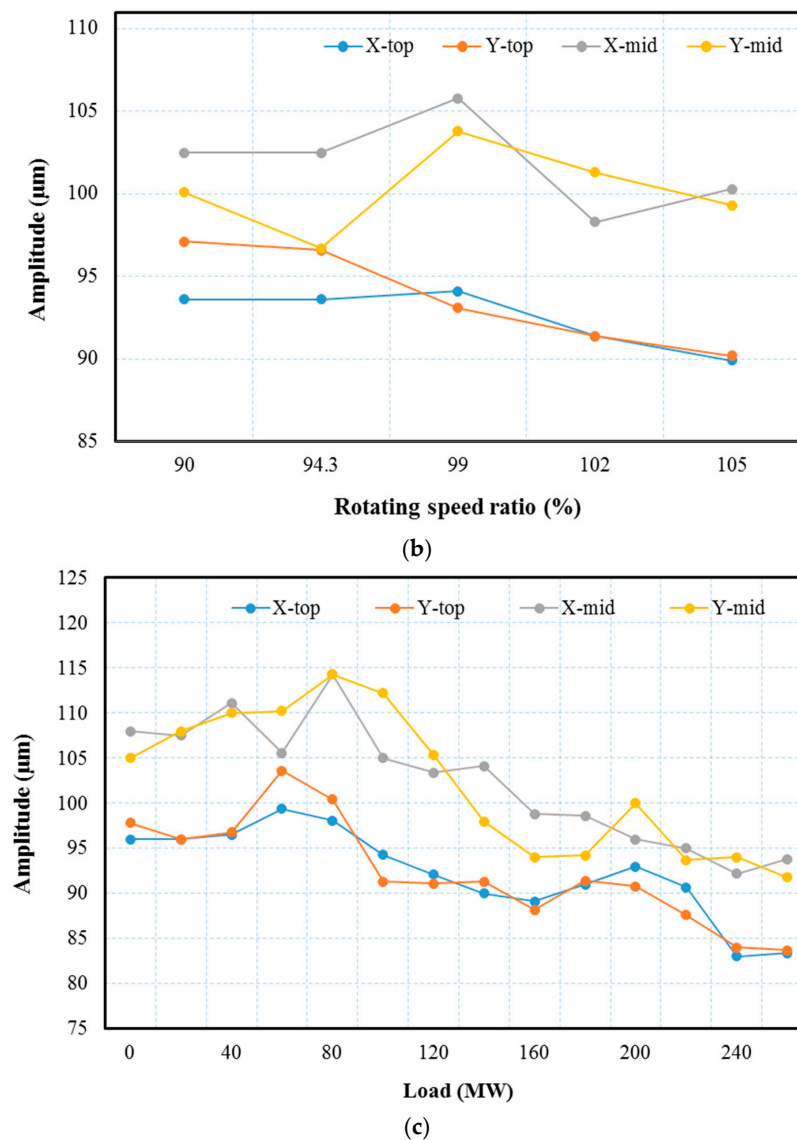


Figure 4. Cont.



**Figure 4.** Vibration peak value of stator frame of experimental tests: (a) excitation test at no-load and rated speed condition; (b) rotation speed test at no-load and 100% excitation condition; and (c) load test at rated speed and 100% excitation condition.

The spectrum of the vibration at the mid of structure under the no-load and 100% excitation condition is shown in Figure 5. The dominant frequency of the vibration is the double rotation frequency  $f_2$  (3.125 Hz). The integral multiple of rotation frequency  $f_1$ , and  $f_3$ – $f_6$  are also significant in the spectrum, and the influence on vibration caused by these harmonic components decreases with the increase of frequency. The minor-amplitude ( $f_7$  and  $f_8$ ) and low-frequency component exist due to the hydraulic vibration passing through the base of stator.

From the experimental results, it can be inferred that the main cause of the excessive vibration is electromagnetic factor. There are many methods to measure the air gap of the hydropower unit [13,14]. However, most of them need pre-installed special sensor. For the other units without pre-installed special sensor, a FE analysis using a 2D-magnetic and 3D-mechanical coupled model has been performed to put a further research.

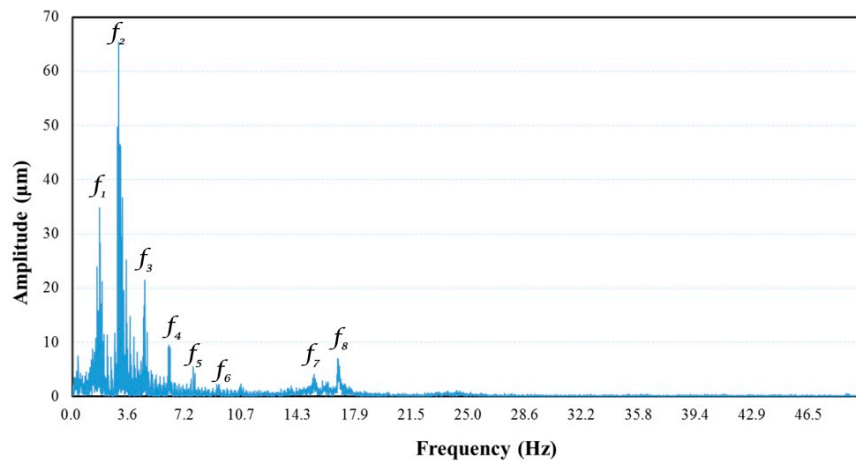


Figure 5. Frequency spectrums of vibration at the mid of stator frame.

### 3. Finite Element Analysis

#### 3.1. Methodology

A 2D-magnetic and 3D-mechanical coupled FE model was established to investigate the stator vibration problem. Firstly, a 2D generator model was built in the commercial software Maxwell for electromagnetic field analysis. Then, the results of electromagnetic analysis were imported in 3D mechanical model as the excitation condition. Finally, comparative analysis with different eccentric models and radial-stud structure model were performed. Figure 6 demonstrates the schematic procedure of the FE analysis.

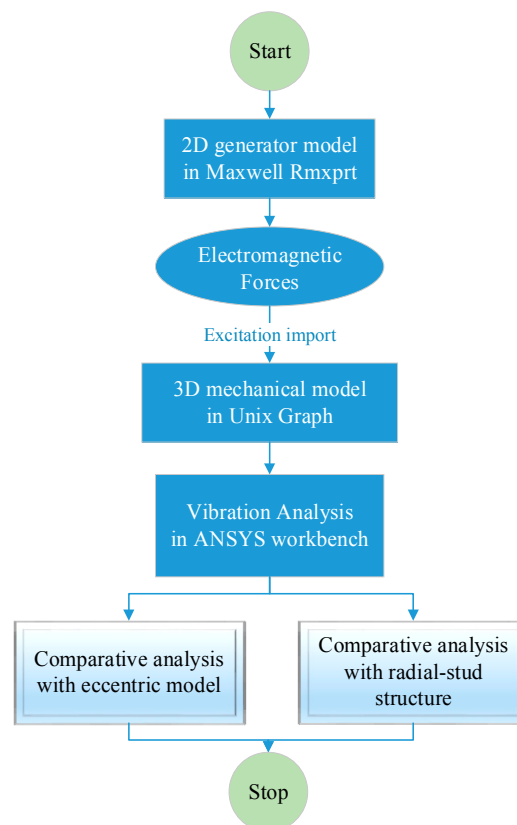


Figure 6. Schematic procedure of finite element (FE) analysis.

### 3.2. A 2D Generator Model for Electromagnetic Analysis

The aim of magnetic field analysis is to acquire the magnetic flux density distribution of the studied hydropower generator and obtain the electromagnetic forces for the following mechanical analysis. Since unacceptable computational time is required for 3D electromagnetic analysis, a 2D FE model with almost equivalent accuracy was established based on an assumption that the magnetic field is constant along the axial direction of the generator. This assumption reduces the degree of freedom in the computation model which would shorten the calculation time significantly. The computational model consists of two parts: Magnetic circuit of the rotor–stator system and external excitation circuit of rotor coil. The basic parameters of the generator are given in Table 1, and the 2D model of electromagnetic analysis is presented in Figure 7.

**Table 1.** Basic parameters of the electromagnetic model.

| Parameter                                  | Value  |
|--|--------|
| Radius of rotor (mm)                       | 6430   |
| Outer diameter of stator (mm)              | 13,700 |
| Inner diameter of stator (mm)              | 12,900 |
| Height of stator core (mm)                 | 2340   |
| No. of parallel branches of stator winding | 4      |
| No. of stator's slots                      | 528    |
| No. of poles                               | 64     |
| Rotate speed (r/min)                       | 93.75  |

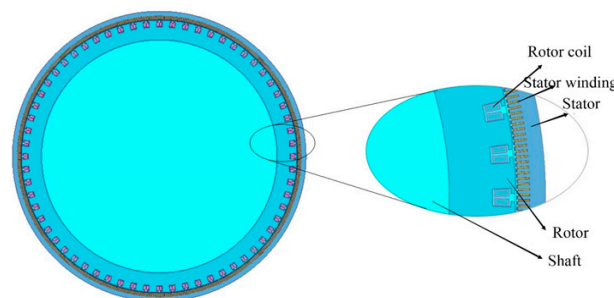


**Figure 7.** 2D model of electromagnetic analysis.

The stator core and rotor core are made of silicon steel 50W250 and its magnetization characteristic is described by the nonlinear B-H curve (B stands for magnetic field intensity, while H represent magnetic induction intensity) which is shown in Figure 8.

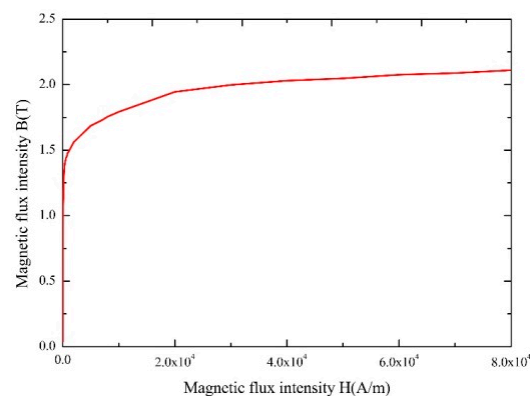


**Figure 8.** B-H (B stands for magnetic field intensity, while H represent magnetic induction intensity) curve of silicon steel 50W250.

The FE simulation of the electromagnetic equation for the magnetic vector potential shows the relation between the magnetic field  $H$  and current density  $J$ , the constitutive laws of the used materials and the formula linking the induction  $B$  and the magnetic vector potential  $A$ .

$$\frac{\partial}{\partial x} \left( v \frac{\partial A}{\partial x} \right) + \frac{\partial}{\partial y} \left( v \frac{\partial A}{\partial y} \right) = J + \sigma \frac{\partial A}{\partial t} \quad (1)$$

where  $v$  is the velocity of moving objects, and  $\sigma$  is the conductivity of the studied region. In this non-linear and time dependent equation, the discretization of the time step needs to be considered.

Electromagnetic forces at the air gap are generated through the interaction between the stator and rotor harmonic fluxes, including their respective fundamental fluxes. Electromagnetic forces due to the Maxwell stress are calculated using the following equation:

$$F_r = \frac{1}{\mu_0} (B_r^2 - B_t^2) \quad (2)$$

where  $\mu_0$  is the permeability of air, and  $B_r$  and  $B_t$  are the flux densities of the radial and tangential components, respectively.

To stabilize the electromagnetic field in a short time, an external electric circuit was utilized to excite the model. In this case, simulations can be carried out under different loads and excitation conditions by changing the resistance and the reactance in the circuit in Figure 9 which is the external circuit built in Maxwell circuit editor. LPhaseA, LPhaseB, LPhaseC represent the three-phase windings of the stator, and RA, RB, RC are the resistance of stator windings. LA, LB, LC are the inductance of the stator coils, while R1, R2, R3 are the load resistance of the generator.

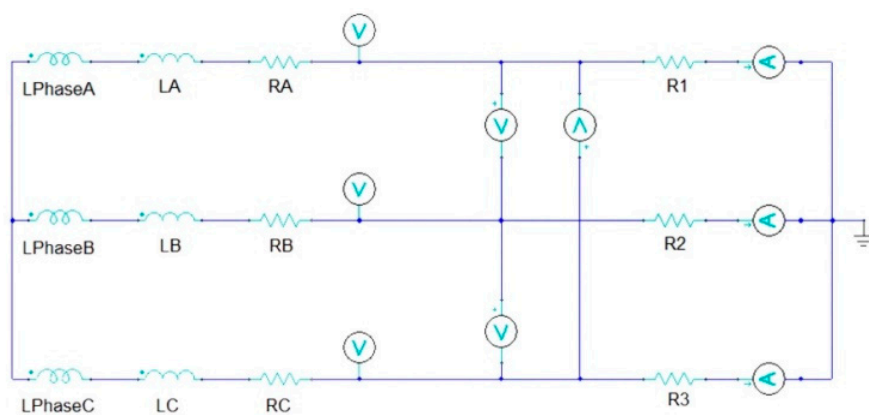


Figure 9. External circuit of hydro-generator.

Meshing the model is crucial for the simulation. The quality of mesh positively affects the accuracy of simulation results while it is restricted by the property of computer. To obtain mesh of higher precision, cut down calculation cost and improve the integration accuracy at the same time, a self-adaptive meshing technique is adopted. Since the shaft of the studied generator is made of non-magnetic material, it has little influence on the analysis. Therefore, the mesh of the shaft is relatively coarse to reduce the calculation amount, while the mesh of magnetic material is of high quality. The mesh near the interface of each part and the mesh along the path of integration are subdivided and optimized (Figure 10). The total number of elements of the computational model is 296,217.

Experimental tests on the studied generator were performed under the same condition. The results of the tests were used to tune the electromagnetic FE models' parameters (including the field current, B-H curve and the wire parameters). Finally, more accurate models with an error of 0.33% which

could be ignored were obtained. Table 2 shows the results comparison between simulation and experimental tests.

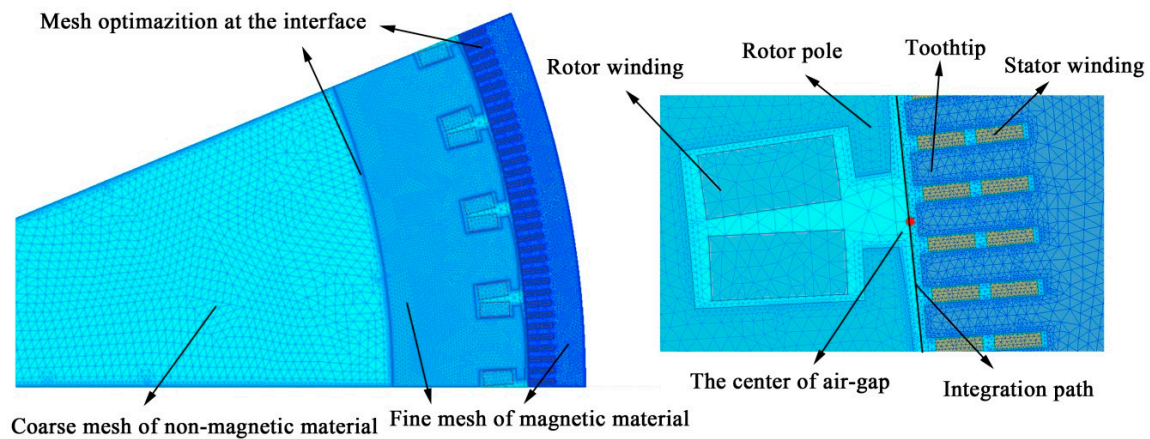


Figure 10. Improved mesh of generator model.

Table 2. The results comparison between simulation and experimental tests.

| Item                 | Simulation | Experiment | Error |
|----------------------|------------|------------|-------|
| Peak of line voltage | 21.87 kV   | -          | -     |
| Peak of line current | 14.72 kA   | -          | -     |
| Voltage              | 15.44 kV   | 15.76 kV   | 2.0%  |
| Current              | 10.41 kA   | 10.1826 kA | 2.2%  |
| Power                | 250.6 MW   | 250.1 MW   | 0.33% |

### 3.3. A 3D Stator Model for Mechanical Analysis

The mechanical structure analysis was conducted on a 3D stator model of the investigated hydropower generator. Based on the principle of conservation of mass and momentum, the computational model can be described by the following equation:

$$\mathbf{M}\ddot{\mathbf{q}} + \mathbf{C}\dot{\mathbf{q}} + \mathbf{K}\mathbf{q} = \mathbf{F}_{hydraulic} + \mathbf{F}_{electromagnetic} + \mathbf{F}_{boundary} \quad (3)$$

where  $\mathbf{M}$ ,  $\mathbf{C}$  and  $\mathbf{K}$  are the matrices of mass, damping and stiffness, respectively.  $\mathbf{F}$  stands for the column vector of external forces.

Since the research is focused on the response of stator frame under the action of electromagnetic forces, the hydraulic disturbance derived from the foundation is ignored.  $\mathbf{F}_{boundary}$  stands for the constraints originated from the bolt connections between stator pack and brackets, which are considered as a fixed support.

The whole model is composed of several sub-domains shown in Figure 3. Each sub-domain was meshed independently and the continuity was enforced by using a Lagrange multiplier technique in the weak form. Three parameters are introduced to describe the mechanical behavior of the material of the studied generator: Poisson ratio, density and Young modulus. Since the stator coils are electrically insulated by a layer of varnish and covered by resin, and the stator core consists of lots of thin sheets with slots for the coils which are compressed into packets, the material of the stator pack cannot be considered to be homogeneous or isotropic, therefore the model of the core is simplified to a cylinder and the coils were modelled as rods with reduced Young's modulus [2]. The material characteristics of the stator model are shown in Table 3.

**Table 3.** Material characteristics.

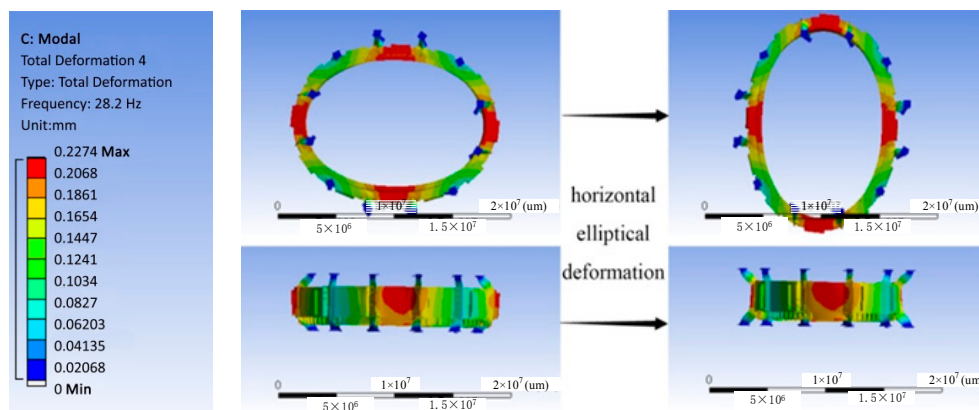
| Item         | Material             | $\rho$ (kg/m <sup>-3</sup> ) | E ( $\times 10^{11}$ Pa) | $\mu$ (-) |
|--------------|----------------------|------------------------------|--------------------------|-----------|
| Stator core  | Silicon steel 50W250 | 7650                         | 1.9                      | 0.28      |
| Coils        | Red Cooper           | 3580                         | 1.5                      | 0.34      |
| Stator frame | Steel Q235A          | 7850                         | 2.1                      | 0.3       |
| Cooler       | Aluminum alloy       | 2770                         | 0.71                     | 0.33      |

When studying the mechanical performance, modal analysis to investigate the inherent property is required at the first place. The constraint at the bottom of the stator system was set as totally fixed support, while the top of the structure was restricted of the displacement in the radial and vertical direction, for the stator is mounted on the base of generator room and fixed to upper generator bracket with bolt connection. The FE model was meshed using Tetrahedrons method, and the body sizing was set as 0.05 m. The total number of elements is 3,781,432.

Several natural frequencies corresponding to different mode were acquired in modal analysis, and the description of the deformation of each mode is given in Table 4. The first order mode-shape of the structure shown in Figure 11 indicates that the vibration forced by low frequency exciting source will be elliptical deformation in the horizontal direction which is in good agreement with the experimental test.

**Table 4.** Description of mode-shapes of the stator pack.

| Mode | Natural Frequency | Description                                 |
|------|-------------------|---|
| 1    | 28.2 Hz           | Horizontal elliptical deformation           |
| 2    | 29.6 Hz           | Horizontal circular displacement            |
| 3    | 41.4 Hz           | Horizontal triangular tensile deformation   |
| 4    | 52.1 Hz           | Horizontal quadrangular tensile deformation |

**Figure 11.** The first order mode-shape of the stator pack at 28.8 Hz.

## 4. Comparative Analyses of Different Models

### 4.1. Eccentric Rotor–Stator Model

#### 4.1.1. Electromagnetic Field Analysis

A concentric model of the hydropower generator has a uniform air gap distributing around the rotor circumference hence the sum of these forces acting on the rotating machine is equal to zero. However, the non-uniform air gap of the eccentric model would distort the distribution of magnetic field and lead to unbalanced radial magnetic force referred as UMP which is the main cause of the electromagnetic vibration.

There are many kinds of eccentricities during practical operations because of manufacturing deviation and assembly error, and it can be classified into three categories: eccentric rotor model with a time-varying air-gap known as dynamic eccentricity, eccentric stator model with a time-invariant air-gap referred as static eccentricity and the coexistence of both static and dynamic eccentricity (Figure 10). Both dynamic and static eccentric models were established in this research.

The air-gap eccentricity parameter  $\delta$  was introduced to describe the level of eccentricity.  $g_0$  represents the normal air gap thickness.  $u$  denotes the distance between the center of rotor and stator centerline. In this paper, the value of  $\delta$  of both dynamic eccentric model and static eccentric model were set to 0.2.

$$\delta = \frac{u}{g_0} \quad (4)$$

Simulations were performed under the no-load and 100% excitation current condition on different models. The results are presented in Figures 12 and 13. Obviously, due to the non-uniform distribution of air-gap, the electromagnetic forces of eccentric model are no longer in equilibrium. They increase near the minimal air gap thickness and decrease near maximal air gap thickness.

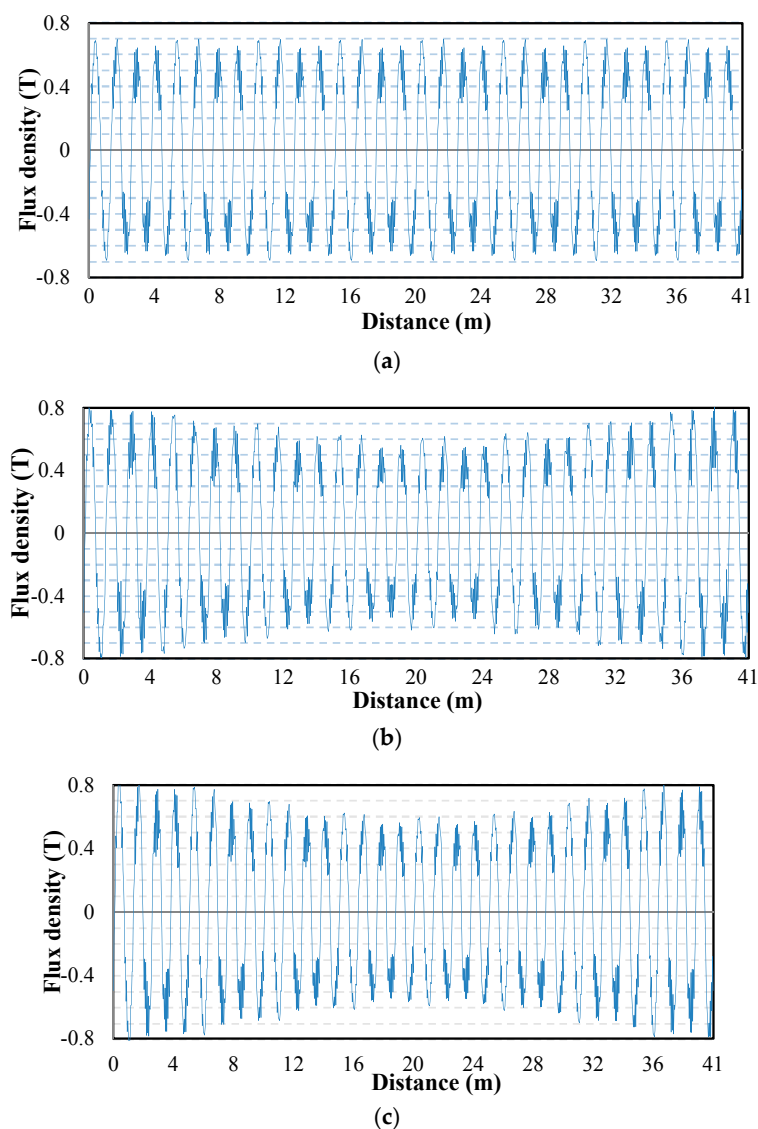


**Figure 12.** Magnetic flux density at the center of air-gap with different eccentric models: (a) concentric model; (b) static eccentric model; and (c) dynamic eccentric model.

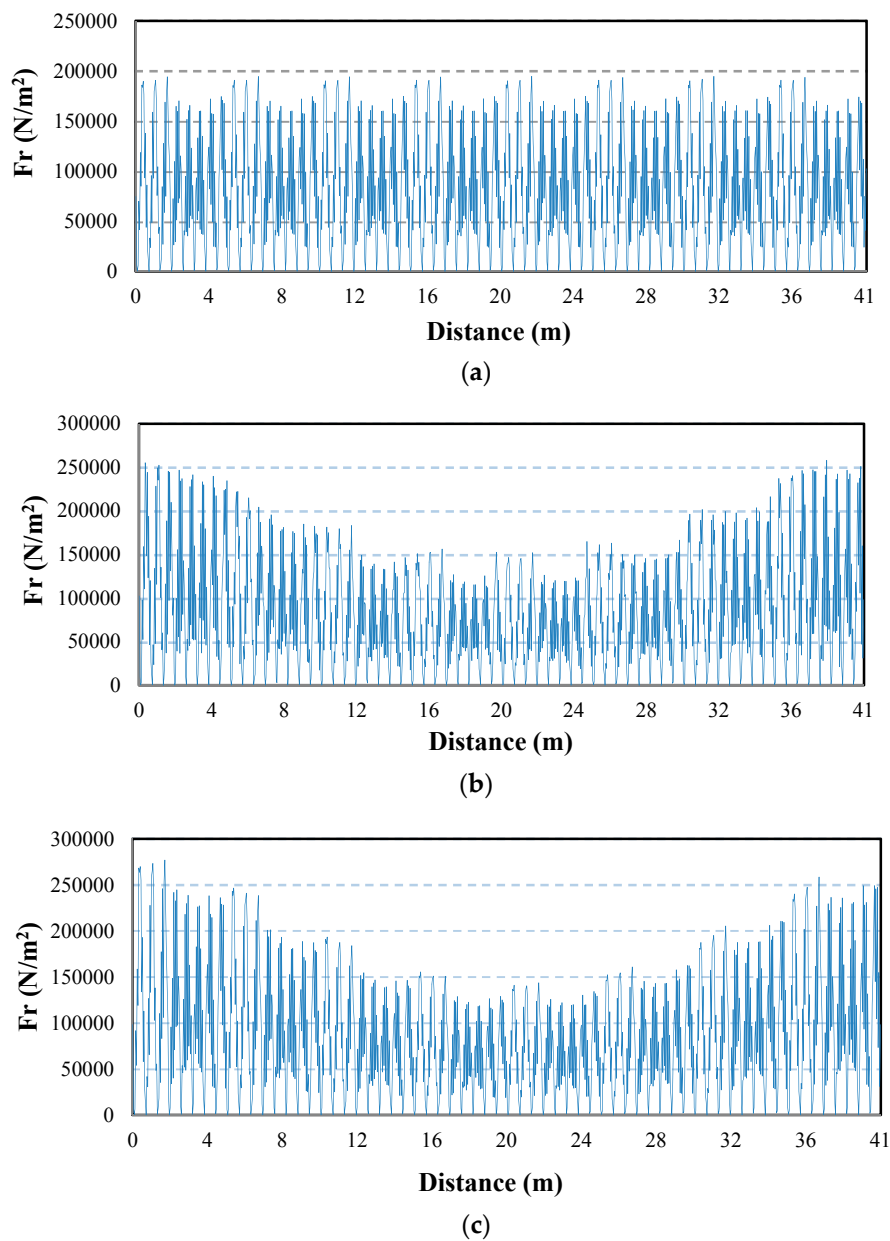


**Figure 13.** Electromagnetic force densities at the center of air-gap with different eccentricity: (a) concentric model; (b) static eccentric model; and (c) dynamic eccentric model.

It can be also observed that there is no obvious difference in distributions of flux density between the static eccentric model and the dynamic eccentric model at the initial time, but the magnetic flux density of the dynamic model is time-varying, so the resultant of electromagnetic forces (UMP) under dynamic eccentric condition have a time-varying direction while the direction of the UMP of the static eccentric model always points to the position where the air gap thickness is minimum.

Spectrum analysis was carried out to investigate the harmonic component of the radial electromagnetic force density of different eccentric model, and results are presented in Figure 14.

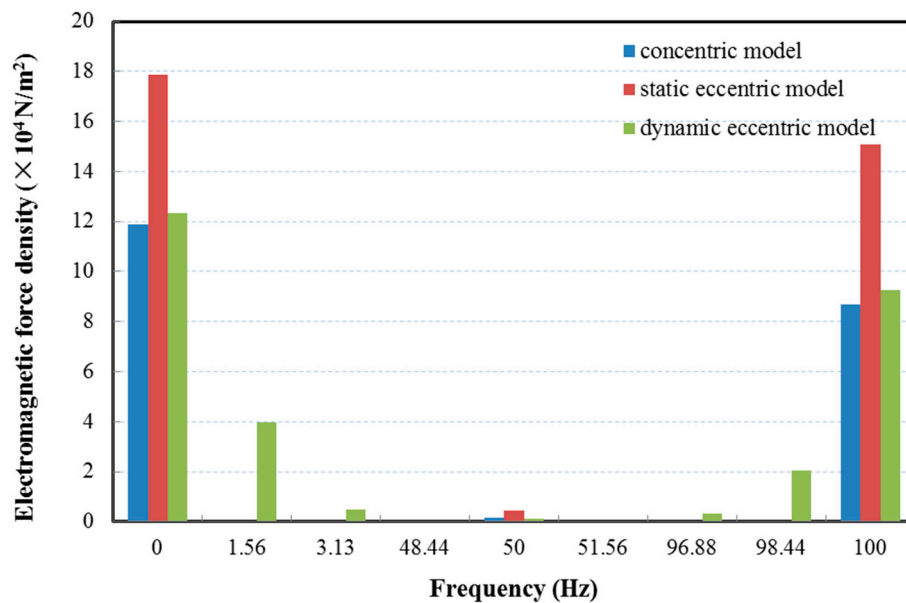


**Figure 14.** Fast fourier transformation (FFT) of electromagnetic force density with different eccentric models.

From the histogram, it can be observed that there is no rotating frequency component in the static eccentric model, and the dominant frequency of the electromagnetic forces of these models with different eccentric conditions are 0 Hz and 100 Hz which can be described in Equation (3), and the other characteristic frequencies produced by the combined effect of both the rotor harmonics and the rotational frequency can be explained in Equation (4):

$$f = 2p \times f_r \times n (n = 0, 1, 2, \dots) \quad (5)$$

$$f_d = f \pm k \times f_r (k = 0, 1, 2, \dots) \quad (6)$$

where  $f$  is the fundamental frequency,  $p$  is the number of pole-pairs,  $f_r$  is the rotational frequency of rotor, and  $f_d$  is the frequency of dynamic eccentricity model.

Integral multiple rotation frequencies observed in FE analysis and the experiment tests indicates that there is a degree of dynamic eccentricity in the rotor–stator system of the generator. Since the electromagnetic forces caused by dynamic eccentricity could augment the vibration significantly, increasing the concentricity and roundness of the rotor–stator system by improving the assembly and manufacturing quality is an effective approach to reduce the vibration. The double rotation frequency, which turns out to be the dominant frequency (Figure 5), is still uninterpretable in this computation model, and it is considered as the consequence of bidirectional coupling effect between rotor and stator.

#### 4.1.2. Transient Structure Analysis

Since the structure is excited by the coexistence of UMP and electromagnetic torque, which is the function of position, eccentricity and time, it is necessary to conduct a transient analysis to reveal the behavior of stator under the action of electromagnetic force. Therefore, a simulation of transient structure analysis is performed under the condition of 100% current excitation and last for 1.29 s which is about twice the period of rotation.

The results of dynamic response of the concentric model and eccentric model are illustrated in Figures 15 and 16. It is clearly shown that the UMP brought by rotor eccentricity augment the vibration significantly. Besides, the displacement of the eccentric model presents apparent periodicity rule. Moreover, the vibration at the mid of stator pack is stronger, which is in a good agreement with the experimental test, because it is relatively far away from the upper boundary constraint. Therefore,

the stiffness at the middle of the structure should be increased and the constraint at the top of the frame needs to be enhanced based on the strong vibration occurs at the upper part of the structure, especially at the middle.

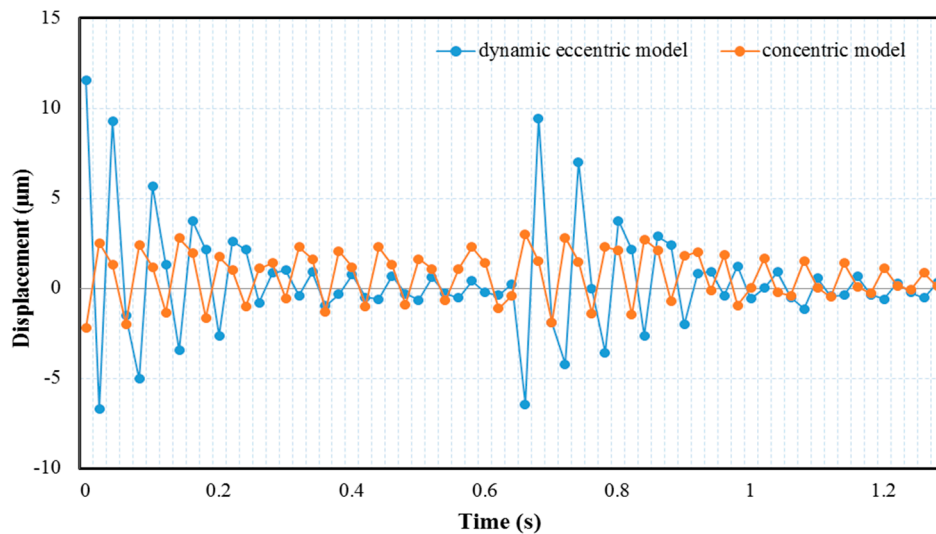


Figure 15. Comparison between concentric model and dynamic eccentric model.

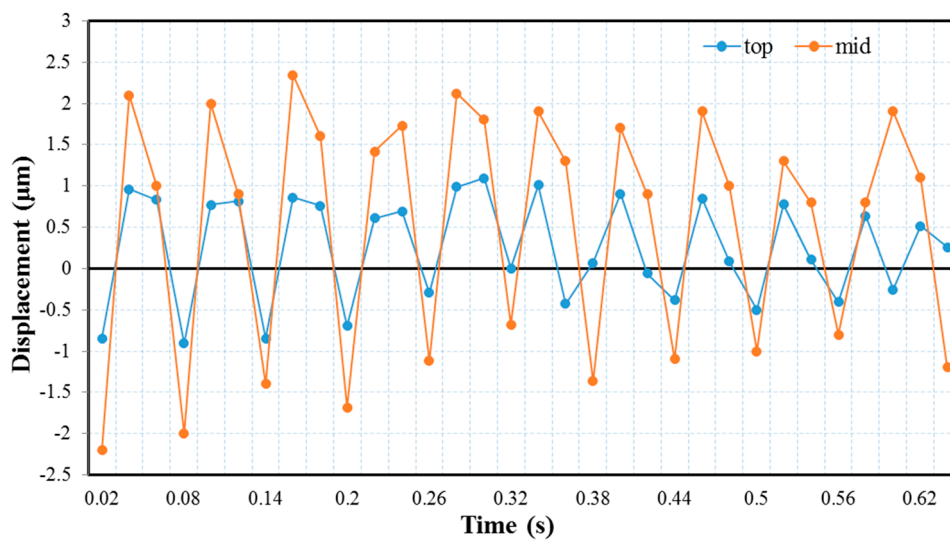


Figure 16. The transient analysis results of concentric model.

#### 4.1.3. Harmonic Response Analysis

Harmonic response analysis is a method to study the steady-state response of structure subjected harmonic load with different frequencies, with which we can calculate the steady-state forced vibration of the structure to predict the dynamic response and to verify whether the designed structure is able to overcome harmful effect caused by resonance and fatigue.

The differential equation of forced vibration of structure under harmonic load condition can be expressed as follows:

$$[M]\{\ddot{X}\} + [K]\{X\} + [C]\{\dot{X}\} = \{F\} \sin(\theta t) \tag{7}$$

Equation (6) shows the displacement response of each node:

$$\{X\} = \{A\} \sin(\theta t + \psi) \tag{8}$$

where  $\{\ddot{X}\}$ ,  $\{\dot{X}\}$ , and  $\{X\}$  indicate the vector of acceleration, velocity and displacement, respectively. Substituting Equation (6) into Equation (5), this following equation can be obtained:

$$\{A\} = [-M\theta^2 \sin(\theta t + \psi) + K \sin(\theta t + \psi) + C\theta(\theta t + \psi)]^{-1} \cdot \{F\} \sin(\theta t) \quad (9)$$

For the purpose of studying the response of the stator model under the action of electromagnetic force, mode superposition method was chosen because of its high accuracy and solution efficiency. Engineering experience shows that the most harmful mechanical vibration often caused by low-frequency component, hence, the solution area is set at 1–40 Hz.

The results of harmonic response analysis in Figure 17 show that: Both static and dynamic eccentricity enlarged the vibration. Besides, the rotor eccentricity augments the vibration significantly. The maximum amplitude occurs at 1.56 Hz (rotating frequency) and the amplitude decreases with the increase of frequency. Moreover, the abnormal enlargement found at 25–30 Hz indicates that the structure could be vulnerable at this area. It is known from the modal analysis that this region is close to the first two orders of natural frequency (28.2 Hz, 29.6 Hz), so it can be inferred that the amplitude increases because of the resonance.

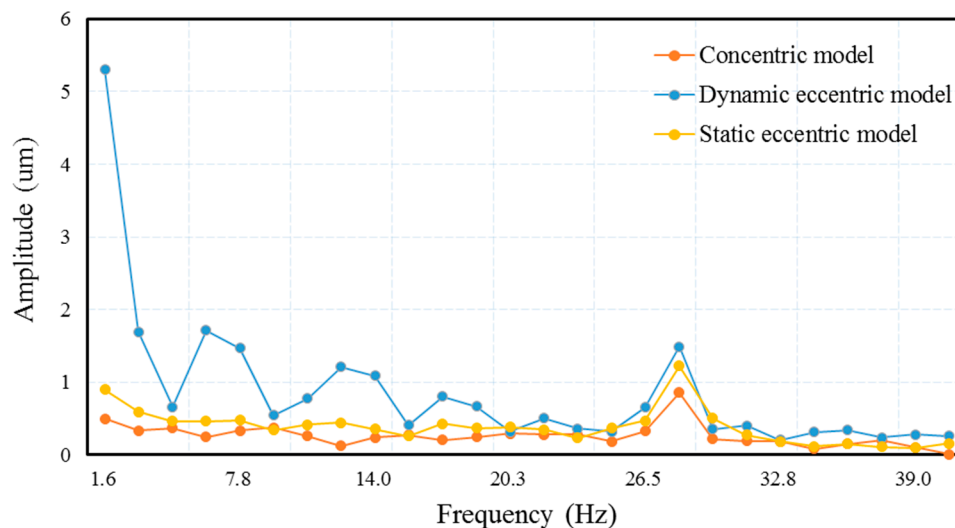


**Figure 17.** The harmonic response of the studied generator.

## 4.2. Structural Comparative Analysis

### 4.2.1. Simulation of Different Structures

Oblique-stud structure is a flexible design to eliminate the negative effect due to the internal force of the stator core thermal expansion and cut down the manufacturing cost at the same time. To investigate the effect of different structures on vibration, comparative simulation test between oblique-stud structure and traditional rigid radial-stud structure presented in Figure 18 (only the direction of the studs is changed) was performed under the rated condition.

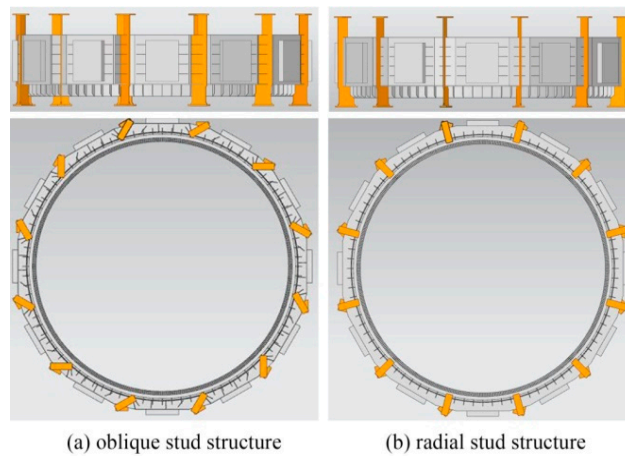


Figure 18. Models of oblique-stud structure and radial-stud structure.

The results presented in Table 5 show that the vibration of the studied oblique-stud structure is obviously stronger under the action of electromagnetic force, and the vibration shape is changed from circular displacement (Figure 19) to elliptical deformation in the horizontal direction (Figure 11).

Table 5. Simulation results of different structures.

| Item                          | The Studied Stator Frame          | Contrast Model                   |
|-------------------------------|-----------------------------------|----------------------------------|
| Structures                    | Oblique-stud structure            | Radial-stud structure            |
| Characteristic                | flexible                          | rigid                            |
| Natural frequency of 1st mode | 28.2 Hz                           | 32.2 Hz                          |
| Description of 1st mode shape | Horizontal elliptical deformation | Horizontal circular displacement |
| Maximum amplitude             | 2.1 μm                            | 1.4 μm                           |

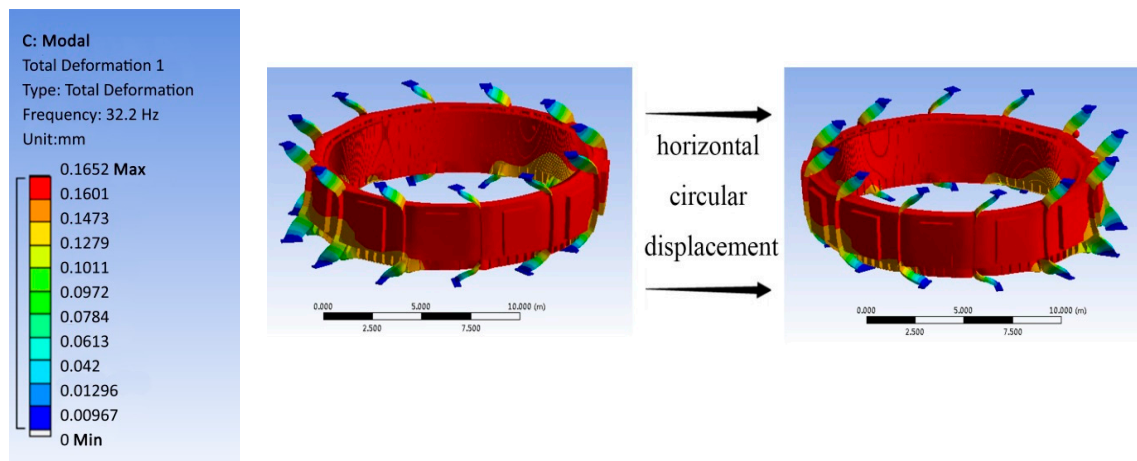


Figure 19. The first order mode-shape of the contrast model at 32.2 Hz.

#### 4.2.2. Research of Different Structures

To confirm the above conclusions, the vibration data of units with different stator frame structures of the same capacity were collected and compared (Table 6).

**Table 6.** Vibration data of stator frame of different units.

| Station      | No. of Unit | Capacity (MW) | Vibration Amplitude ( $\mu\text{m}$ ) | Type     |
|--------------|-------------|---------------|---------------------------------------|----------|
| Three Gorges | 15          | 700           | 18                                    | rigid    |
|              | 24          | 700           | 50                                    | flexible |
| Laxiwa       | 1           | 700           | 120                                   | flexible |
| Goupitan     | 3           | 600           | 60                                    | rigid    |
|              | 4           | 600           | 200                                   | flexible |
| pubugou      | 1           | 600           | 6                                     | rigid    |
|              | 4           | 600           | 28                                    | rigid    |

Despite the measurement error, quality difference of installation and manufacturing, structural difference, the statistical results show that the vibration of the rigid structure is obviously smaller, and it is found that the vibration amplitudes of the units with flexible design and large vibration have a significant relationship with the excitation condition: the vibration grows stronger with the increase of the excitation current.

It can be concluded that the oblique-stud structure can be characterized by large elasticity and small rigidity, which determines that it is relatively vulnerable when suffering electromagnetic forces. Thus, it is necessary to take precautions, such as increasing the thickness of oblique-stud, strengthening the connection between the stator frame and brackets, to avoid electromagnetic vibration.

## 5. Conclusions

In this paper, field experimental tests and FE analysis using a 2D-electromagnetic and 3D-mechanical coupled computational model were conducted on an oblique-stud stator frame of a large hydropower generator that experiences undesirable vibration during practical operations. Both the experimental test results and simulation results show that the vibration is caused by electromagnetic factors, and the vibration grows stronger with the increase of the excitation current. Further study was performed to find the cause of the vibration through comparative simulation analyses, and optimization strategies to reduce the vibration of stator frame were proposed.

**Acknowledgments:** This work was supported by the National Key R & D Program of China (Nos. 2016YFC0402205 and 2016YFC0401910) and the National Natural Science Foundation of China (NSFC) (No. 51079057 and No. 51239004).

**Author Contributions:** Xuanlin Peng and Jianzhong Zhou conceived and designed the experiments, Yanhe Xu and Diyi Chen performed the simulations; Ruhai Li analyzed the data; and Xuanlin Peng and Han Liu wrote the paper.

**Conflicts of Interest:** The authors declare no conflicts of interest.

## References

- Martinez, J.; Belahcen, A.; Detoni, J.G. A 2D magnetic and 3D mechanical coupled finite element model for the study of the dynamic vibrations in the stator of induction motors. *Mech. Syst. Signal Process.* **2016**, *66–67*, 640–656. [[CrossRef](#)]
- Donát, M.; Dušek, D. Eccentrically mounted rotor pack and its influence on the vibration and noise of an asynchronous generator. *J. Sound Vib.* **2015**, *344*, 503–516. [[CrossRef](#)]
- Sathyan, S.; Belahcen, A.; Kataja, J.; Vaimann, T.; Sobra, J. Computation of Stator Vibration of an Induction Motor using Nodal Magnetic Forces. In Proceedings of the 2016 XXII International Conference on Electrical Machines, Lausanne, Switzerland, 4–7 September 2016.
- Bazan, G.H.; Scalassara, P.R. Stator fault analysis of three-phase induction motors using information measures and artificial neural networks. *Electr. Power Syst. Res.* **2017**, *143*, 347–356. [[CrossRef](#)]
- Glowacz, A.; Glowacz, W.; Glowacz, Z.; Kozik, J. Early fault diagnosis of bearing and stator faults of the single-phase induction motor using acoustic signals. *Measurement.* **2017**, *113*, 1–9. [[CrossRef](#)]

6. Lashkari, N.; Poshtan, J.; Azgomi, H.F. Simulative and experimental investigation on stator winding turn and unbalanced supply voltage fault diagnosis in induction motors using Artificial Neural Networks. *ISA Trans.* **2015**, *59*, 334–342. [[CrossRef](#)] [[PubMed](#)]
7. Dorrell, D.G.; Smith, A.C. Calculation of UMP in induction motors with series or parallel winding connections. *IEEE Trans. Energy Convers.* **1994**, *9*, 304–310. [[CrossRef](#)]
8. Smith, A.C.; Dorrell, D.G. Calculation and measurement of unbalanced magnetic pull in cage induction motors with eccentric rotors. *IEEE Proc. Electr. Power Appl.* **1996**, *143*, 193–201. [[CrossRef](#)]
9. Guo, D.; Chu, F.; Chen, D. The unbalanced magnetic pull and its effects on vibration in a three-phase generator with eccentric rotor. *J. Sound Vib.* **2002**, *254*, 297–312. [[CrossRef](#)]
10. Fonteyn, K.; Belahcen, A.; Kouhia, R.; Rasilo, P.; Arkkio, A. FEM for Directly Coupled Magneto-Mechanical Phenomena in Electrical Machines. *IEEE Trans. Magn.* **2010**, *46*, 2923–2926. [[CrossRef](#)]
11. Lin, R.; Arkkio, A. 3-D Finite Element Analysis of Magnetic Forces on Stator End-Windings of an Induction Machine. *IEEE Trans. Magn.* **2008**, *44*, 4045–4048.
12. Xu, Y.; Li, Z. Computational Model for Investigating the Influence of Unbalanced Magnetic Pull on the Radial Vibration of Large Hydro-Turbine Generators. *J. Vib. Acoust.* **2012**, *134*. [[CrossRef](#)]
13. Talas, P.; Toom, P. Dynamic Measurement and Analysis of Air Gap Variations in Large Hydroelectric Generators. *IEEE Trans. Power Appar. Syst.* **1989**, *PAS-102*, 3098–3106. [[CrossRef](#)]
14. Adamowski, J.C.; Souza, A.T.; Pérez, N.; Lima, A.A.; Oda, P.D.; Tiba, H.H. Ultrasonic dynamic air-gap monitoring system for large hydro-generators. In Proceedings of the 2013 IEEE International Ultrasonics Symposium, Prague, Czech Republic, 21–25 July 2013.



© 2017 by the authors. Licensee MDPI, Basel, Switzerland. This article is an open access article distributed under the terms and conditions of the Creative Commons Attribution (CC BY) license (<http://creativecommons.org/licenses/by/4.0/>).